

6

4460

4461

Improved RPC investigation and preliminary electronics studies

4462

4463 The extension in the endcap of the RPC sub-system towards higher pseudo-rapidity will bring the
4464 new detectors to be exposed to much more intense background radiations due to the proximity of the
4465 detectors with the beam line (Figure 4.5). The challenge will be to produce high counting rate de-
4466 tectors with limited ageing rate to ensure a stable operation of the detector over a period longer than
4467 ten years. In Chapter ?? was discussed the influence of the detector design (number and thickness
4468 of gas volumes, OR system, etc...) on the charge deposition and rate capability. Nevertheless, this
4469 question can also be addressed from the electronics point of view as a better signal-to-noise ratio
4470 would also mean the possibility to greatly lower the charge threshold on the signals to be detected,
4471 allowing to use the detector at lower gain, hence lowering the charge deposition per avalanche in the
4472 gas volume. Cardarelli showed that the production of low-noise fast FEEs could help decreasing the
4473 charge deposition per avalanche at working voltage by an order of magnitude, virtually increasing
4474 the life expectancy of such a detector in the same way [281].

4475

6.1 FEE candidates for the production of iRPCs

4476 The extension of the third or fourth endcap disks with improved RPCs has been presented in
4477 Chapter ?? together with the expected background levels (Figure 4.18). An important piece of
4478 these iRPCs will be the Front-End Electronics that will equip the chambers. A fast, low-jitter and
4479 low-charge sensitive electronics will help reducing further the charge deposition in the detector by
4480 making it possible to operate at lower gain.

4481

In the context of the CMS Muon Upgrade, two FEE solutions have been considered to equip the
4482 iRPCs. The baseline for the RPC upgrade is based on the PETIROC ASIC, initially for Time-of-
4483 flight (ToF) applications. A back-up solution is also under study and focusses on a new low-noise
4484 preamplifier designed in INFN laboratories in Rome to replace the preamplification stage of the
4485 already existing CMS RPC Front-End Board.

4486 The FEEs that are foreseen to equip the new RPCs need to be able to detect charges as small as
 4487 10 fC. Not only the new electronics need to be fast and reliable, they also should be able to sustain
 4488 the high radiation the detectors will be subjected to in the region closest to the beam.

4489 6.1.1 CMS RPCROC: the RPC upgrade baseline

4490 Designed by Weeroc, a spin-off company from the french OMEGA laboratory, the PETIROC 2A
 4491 consists in a fast and low jitter 32-channel ASIC originally developed to read-out Silicon Photomul-
 4492 tiplier (SiPM) in ToF applications and that allows for precise time measurements [257, 258]. The
 4493 ASIC uses an AMS 350 ns SiGe technology. The block diagram of the ASIC is showed on Fig-
 4494 ure 6.1. A 10-bit DAC allows to adjust the trigger level in a dynamical range spanning from 0.5 to
 4495 a few tens of photoelectrons and a 6-bit DAC to adjust the response of each individual channel to
 4496 similar a level.

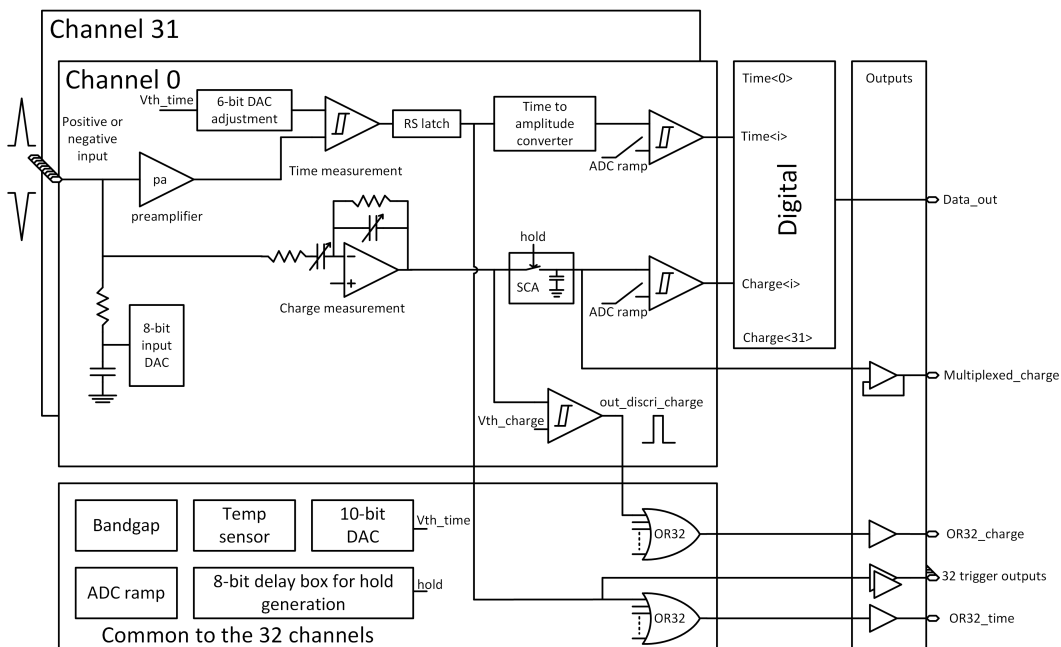


Figure 6.1: PETIROC 2A block diagram.

4497 Nevertheless, in order to adapt this ASIC to CMS, modifications were brought to the PETIROC [177]
 4498 and not all its functions will be used [282]. In the new CMS RPCROC, showed in Figure 6.2, the
 4499 measurement of the charge will be performed by a Time-over-Threshold (ToT) technic, taking profit
 4500 of the capacity the ASIC has in measuring both the leading and trailing edges of the input signals.
 4501 The dynamic range will be expanded towards lower values to allow for the detection of charges as
 4502 low as 10 fC. Due to the radiation levels that are foreseen at the level of the iRPCs, the SiGe tech-
 4503 nology will be replaced by the Taiwan Semiconductor Manufacturing Company (TSMC) 130 nm
 4504 CMOS, to increase its radiation hardness while keeping fast pre-amplification and discrimination
 4505 with a very low jitter that can reach less than 20 ps if no internal clock is used, as can be seen from
 4506 Figure 6.3. The ASIC is associated with an FPGA which purpose is to measure time of the signals.
 4507 The FPGA is equipped with a TDC with a time resolution of 50-100 ps developed by Tsinghua

4508 University. The full system will provide a measurement of the signal position along the strip with a
 4509 precision of a few cm by measuring the signal timing on both ends of the strips.



Figure 6.2: View of the RPCROC Front-End Electronics in which the PETIROC 2A ASIC is visible as well as the FPGA on which the TDC is hosted.

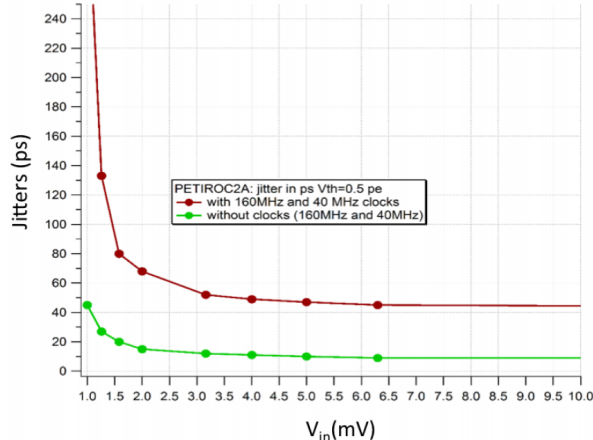


Figure 6.3: The PETIROC time jitter as a function of the input signal amplitude, measured with and without internal clocks.

4510 In order to read-out all 96 strips, 3 ASICs and 3 TDCs, each having an increased number of 64-
 4511 channels, are hosted on a FEB attached to the chamber. Two scenarios are being studied to connect
 4512 the ASICs to the read-out strips [282]. The corresponding read-out panels are showed in Figure 6.4.

4513 On the one hand there is the possibility to design a standard trapezoidal strip panel and to directly
 4514 connect the strips to the ASICs using coaxial cables of similar impedance than the strips. On the other hand,
 4515 the return lines could be embedded directly in extra layers of the strip panel to offer the possibility to
 4516 minimize the amount of on-detector cables by using a single connector to send the signals to the FEB's inputs.
 4517 The first version of the panel is referred to as *coaxial design* while the second as *return design*. In the case of the
 4518 return design panel, the read-out area is a little smaller than in the case of the coaxial panel. This was motivated by
 4519 the need to shield the return strips beneath the copper ground plane visible on the side of the PCB.
 4520

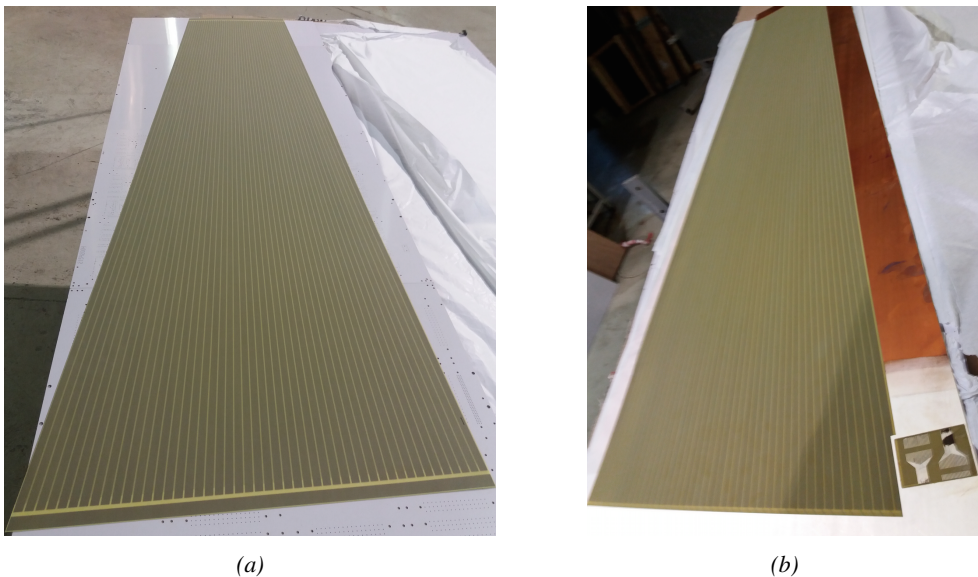


Figure 6.4: View of the coaxial design (Figure 6.4a) and of the return design (Figure 6.4b) of read-out panels used in the iRPC prototypes. Only half PCBs with 48 strips are showed.

4521 6.1.2 INFN Front-End Board: a robust back-up solution

4522 Even though the baseline for the electronics that will equip the iRPCs will be the CMS RPCROC, a
 4523 back-up solution needs to be certified. The back-up has been found in a Front-End Electronics fea-
 4524 turing a fast and low-noise ($1000 e^-$ rms) Silicon (Si) preamplifier and a Silicon-Germanium (SiGe)
 4525 discriminator [283] associated with an optimized read-out panel [284]. The low-noise preamplifier is
 4526 a new version of a preliminary production of a SiGe preamplifier by the team of Cardarelli working
 4527 with INFN Roma with the purpose of equipping the new generation of ATLAS RPCs [285].

4528 The FEB is equipped with eight channels of preamplifiers using a Bipolar Junction Transis-
 4529 tor (BJT) technology and two discriminator ASICs of four channels using Hetero Junction bipolar
 4530 Transistor (HJT) technology. The input signals are amplified at an amplification factor of 0.2 to
 4531 0.4 mV/fC and are then discriminated with a threshold of 0.5 mV at minimum. For each channel,
 4532 the LVDS output is proportional in width to the Time-over-Threshold in the discriminator of the am-
 4533 plified signal with a minimum width of 3 ns. This method allows for an estimation of the avalanche
 4534 charge as the width of the signals usually is consistent and proportionnal to the amount of charge
 4535 released in the gas volume.

4536 The read-out panel features 96 trapezoidal copper strips and has a similar design to the read-out

⁴⁵³⁷ panels used for the CMS RPCROC. As for now, the strips are only read-out from one end.

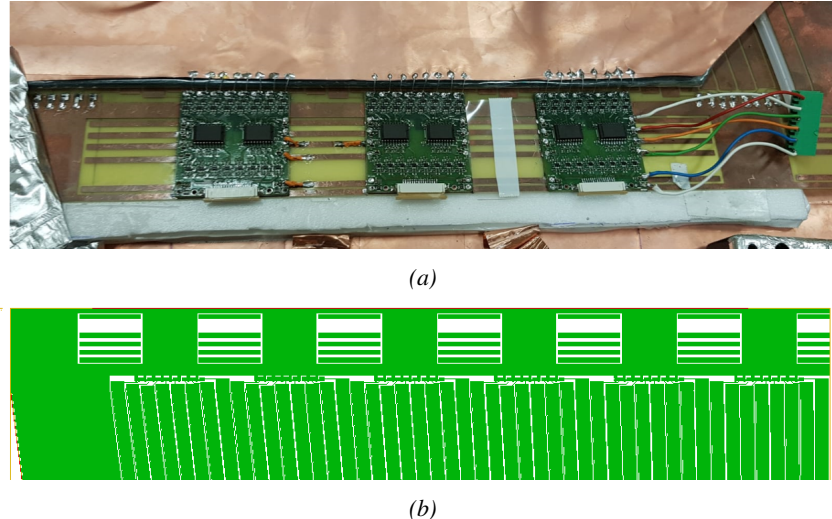


Figure 6.5: Experimental setup used to test the INFN preamplifier with respect to the CMS FEEs.

⁴⁵³⁸ **6.2 Preliminary electronics tests at CERN**

⁴⁵³⁹ **6.2.1 INFN preamplifiers as upgrade candidates**

⁴⁵⁴⁰ INFN electronics were the first ones to be tested by CMS RPC group in collaboration with colleagues
⁴⁵⁴¹ from INFN Roma working in the ATLAS RPC group. The tests with CMS RPCs were performed in
⁴⁵⁴² February 2013 outside of the old GIF facility presented in Chapter 5.1.1. Four preamplifier channels
⁴⁵⁴³ were lended by Cardarelli to equip four CMS RPC channels as presented in Figure 6.9. They were
⁴⁵⁴⁴ directly connected to the strips for the signals induced by muons passing through the gas volume of
⁴⁵⁴⁵ the chamber to be amplified. The output was then sent to a discriminator to digitize the signals and
⁴⁵⁴⁶ filter out the noise by tuning the threshold level. The NIM quad discriminator 821 manufactured by
⁴⁵⁴⁷ LECROY used during this experiment only allows at minimum to set the threshold at a voltage of
⁴⁵⁴⁸ approximately 30 mV on the input signals. Thus, two values of discrimination were used (~ 75 mV
⁴⁵⁴⁹ and ~ 30 mV).

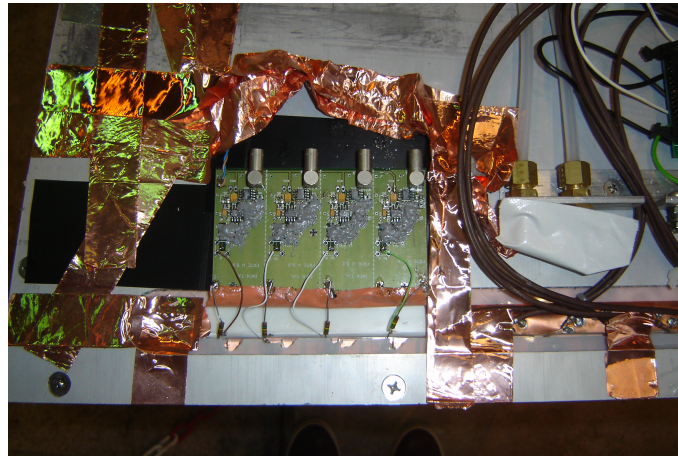
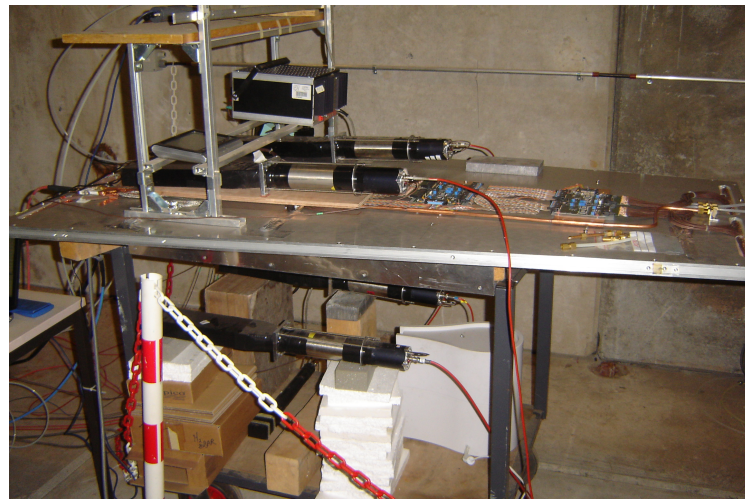


Figure 6.6: The four channels of INFN preamplifiers are mounted directly on a CMS RPC and connected to the four outermost read-out strips of the detector.

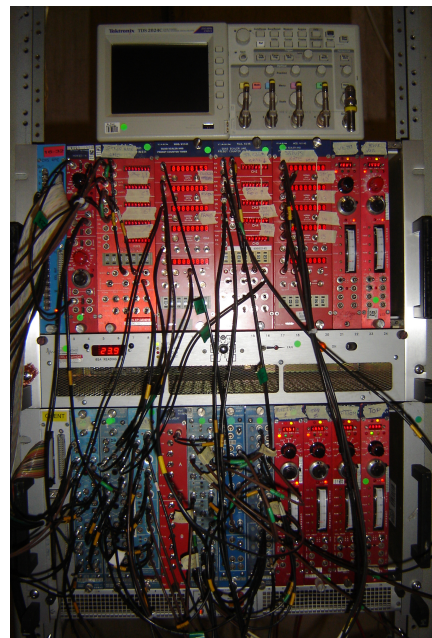
4550 The performance of the chamber equipped with these new preamplifiers was compared to the
4551 performance of CMS FEEs. The experimental setup used is described in Figure 6.7. PMTs a little
4552 less wide than four strips were used to trigger the data taking. Two pairs were used in coincidence
4553 on both the strips connected to the INFN preamplifiers and to the ones connected to the CMS FEEs.
4554 An extra PMT, placed perpendicularly to the rest of the setup at the bottom of the setup was used
4555 to detect potential showers and send VETO signals if necessary. A last PMT was used close to the
4556 power supplies to measure and discard signals due to electromagnetic noise and is not visible on
4557 the pictures. Finally, after discrimination, the output of the INFN preamplifiers together with the
4558 signals from the CMS FEEs were sent to scalers to count the detected signals versus the number of
4559 trigger coincidences as no DAQ software was available at the time. The full pulse processing for this
4560 experiment is shown in Figure 6.8.



(a)



(b)



(c)

Figure 6.7: Experimental setup used to test the INFN preamplifier with respect to the CMS FEEs.

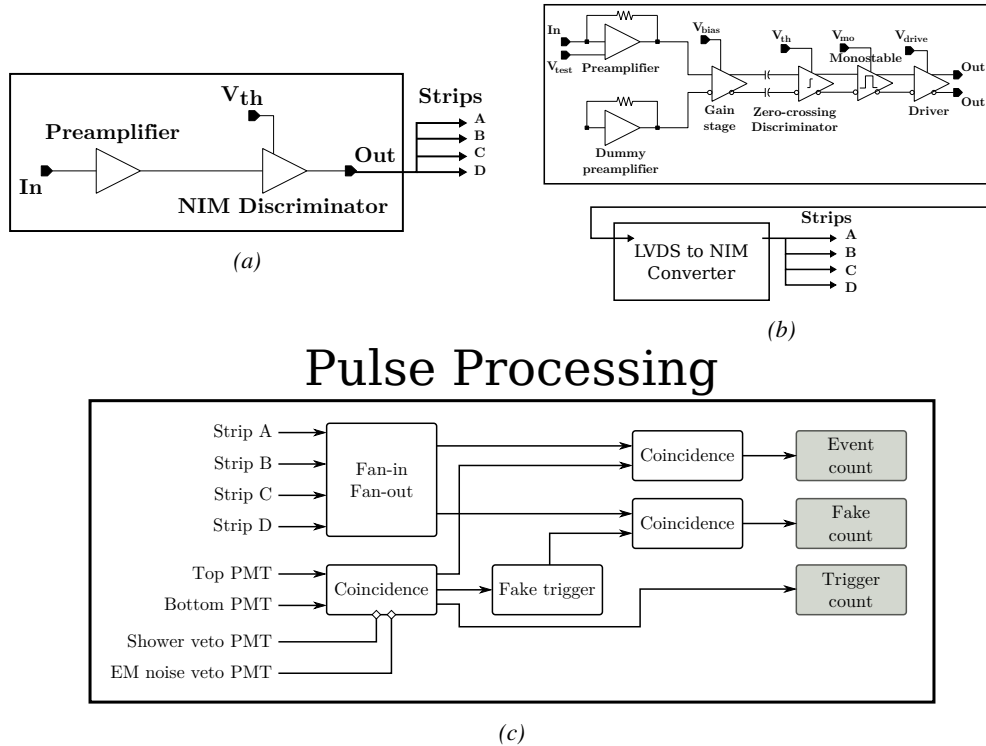


Figure 6.8: The block diagrams corresponding to the signal treatment for both INFN preamplifier (Figure 6.8a) and CMS FEEs (Figure 6.8b) are shown. The digitized signals are then counted in coincidence with the trigger signals provided by PMTs (Figure 6.8c).

4561 The data taking program consisted in High Voltage scans. A first point was taken at 0 V to only
 4562 measure noise. Then the HV was increased to an applied value of 7 kV. The voltage was increased
 4563 in steps of 500 V until 8 kV from where it was increased in steps of 100 V until an upper limit of
 4564 10 kV. After rising the voltage over the electrodes of the RPC, a waiting period of 15 minutes was
 4565 observed to leave time to the electrodes to charge and to the currents to stabilize. The currents were
 4566 reported at the moment the data taking was started. At each HV step, except at 0 V, approximatively
 4567 300 triggers were taken to estimate the efficiency of the detector by counting the number of hits in the
 4568 system (A or B or C or D), referring to the strips. The noise rate per unit area was measured during
 4569 the first 100 s of data taking by counting the number of hits received in each read-out strip. The
 4570 cluster size, the average number of adjacent strips fired during a muon event, could not be measured
 4571 due to the lack of available scalers.

4572 During the data acquisition, in addition to counting the number of signals with respect to the
 4573 number of triggers, the current or the noise rate per unit area as a function of the increasing voltage,
 4574 the environmental parameters were monitored. Using the information provided by a humidity and
 4575 temperature sensor on the gas input line together with the environmental pressure given by a weather
 4576 station, the applied voltage could be corrected following Formula 3.27. Moreover, the voltage line
 4577 was filtered to prevent noise and higher currents in the RPC under test.

4578 The results of the preliminary tests are presented in Figure 6.9. More details on the fit performed
 4579 on the data are provided in Table 6.1. As can be seen, being able to use electronics with a much
 4580 higher sensitivity allows for a HV shift of up to 475 V with a threshold as low as 3 fC corresponding

to the lowest threshold available on the discriminator modules. On the other hand, the higher charge sensitivity also brings a higher noise level. After a first series of measurement performed with a bad grounding leading to grounding loops and hence an artificially higher noise, it can be concluded that the noise rate per unit area of such electronics is approximately one of manitude higher than the noise rate measured with the CMS FEB. The noise reaches approximately 2 Hz/cm^2 at the level of the working in the case of the INFN preamplifier while it is lower than 0.2 Hz/cm^2 for the CMS FEB. It is likely that the higher sensitivity also brings a higher sensitivity to local discharges happening in the gas due to fluctuations of the electric field. The surface of the electrodes not being perfectly smooth, the local electric field may vary quickly. The gas molecules circulating in the gas could then be ionised by the fast variation of the field and trigger an avalanche that can then be detected. Reducing the noise rate per unit area would then come from an improvement of the detector itself rather than from a reduction of the electronic noise of the INFN preamplifier.

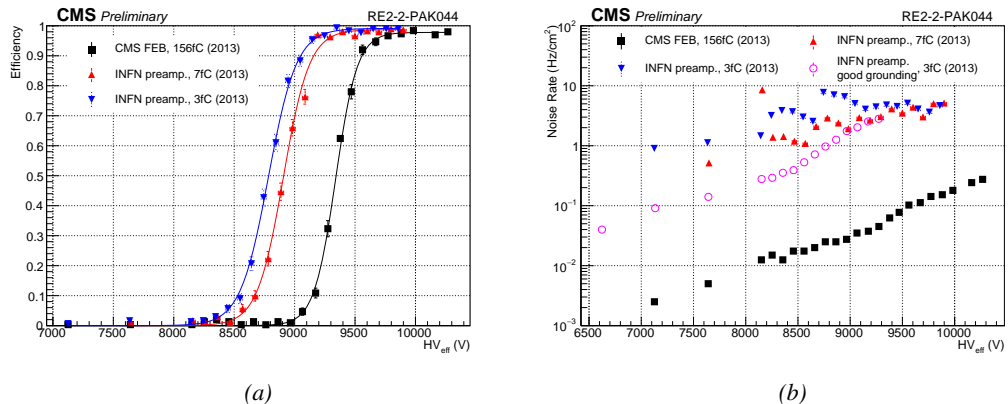


Figure 6.9: Efficiency (Figure 6.9a) and noise rate per unit area (Figure 6.9b) of the CMS RE2-2 detector tested with the standard CMS FEBs (black) and with the INFN preamplifier at different thresholds (red and blue). An extra HV scan was performed with better conditions to measure the noise with a threshold of 3 fC on the INFN preamplifiers.

Data	ϵ_{max}	$\lambda (\times 10^{-2} \text{ V}^{-1})$	HV_{50} (V)	ϵ_{WP}	HV_{WP} (V)
CMS FEB, 156fC (2013)	(0.978 ± 0.004)	(1.12 ± 0.07)	(9339 ± 11)	(0.97 ± 0.01)	(9752 ± 27)
INFN preamp., 7fC (2013)	(0.987 ± 0.003)	(0.93 ± 0.05)	(8907 ± 11)	(0.97 ± 0.01)	(9374 ± 27)
INFN preamp., 3fC (2013)	(0.991 ± 0.003)	(0.86 ± 0.04)	(8783 ± 11)	(0.98 ± 0.01)	(9276 ± 27)

Table 6.1: Results of the sigmoid fit (Formula 3.24) performed on the data presented in Figure 6.9a. The working point and its corresponding efficiency are computed using Formulas 3.24 and 3.25.

6.2.2 INFN preamplifiers mounted onto CMS Front-End Board

Following the first experiment performed in the experimental hall aside of the old GIF, a new series of tests has been done in the CMS RPC assembly laboratory at CERN. For this purpose, the preamplifiers have been designed to be standalone single channels. To have a consistent comparison with the CMS FEB, a FEB prototype has been built based on the current CMS design. As shown in Figure 6.10, the preamplifiers are meant to be plugged in one of the available 16 channels of the board that produces an LVDS output with similar characteristics than the CMS FEB.

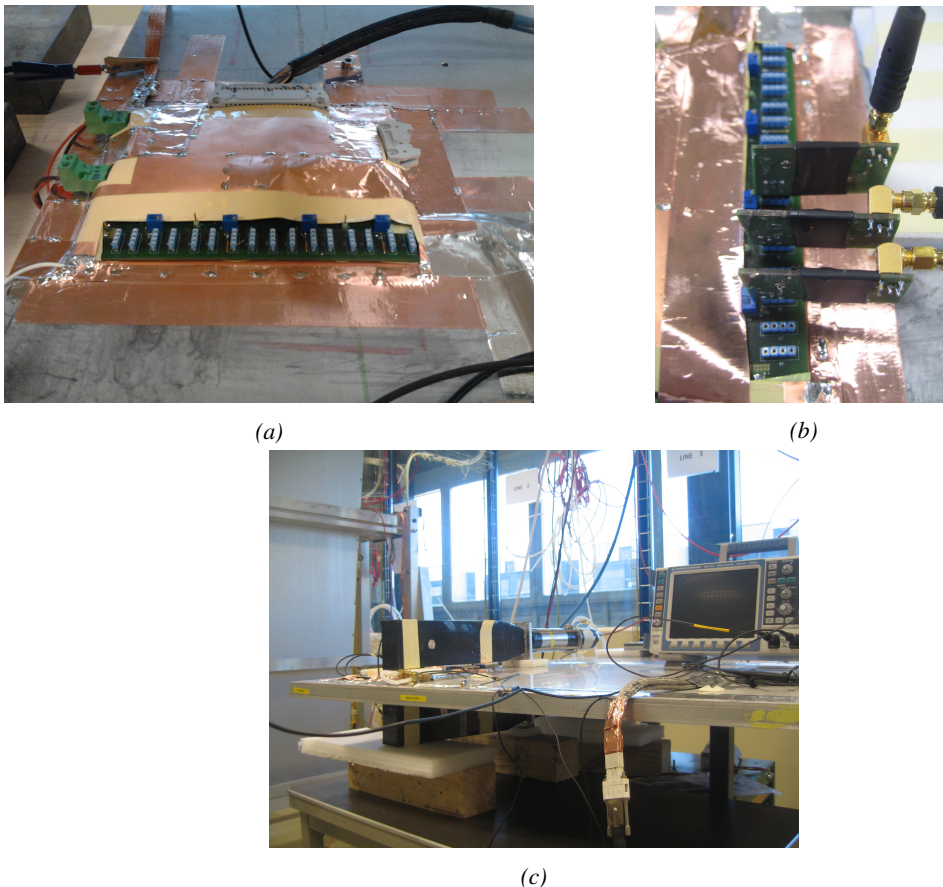


Figure 6.10: Figure reffig:Setup-INFN-904:A: Shielded Front-End Board on which the INFN preamplifiers are to be mounted. Figure reffig:Setup-INFN-904:B: Three INFN preamplifiers connected onto the test FEB. Figure reffig:Setup-INFN-904:C: Experimental setup used to test the INFN preamplifier single mounted on a FEB similar to the CMS FEB.

At the time of the second experiment, only three channels could be lent by the team of INFN Roma. The impedance of the preamplifiers was set to $100\ \Omega$ at delivery. The strips are then connected to the preamplifiers using $50\ \Omega$ coaxial cables equipped with SMC connectors, known for their good transmission. To match the impedance of the preamplifier input with the signal cable, a $100\ \Omega$ resistor was added in parallel of the input line. In CMS endcap RPCs, the strips are left floating. For the purpose of this test, it was necessary to terminate the strips on both ends to prevent reflections in the transmission line. The impedance of the strips being approximately $25\ \Omega$, the strips were terminated with $50\ \Omega$ resistors on the signal cable side, and with $25\ \Omega$ resistors on the end side.

The threshold of the zero-crossing discriminators used on the FEB is controlled via a labview interface similar to the one used to control the threshold of the CMS FEB. Various thresholds were used in a range in between 7 and 5 fC. These values are a little higher than the minimal threshold of about 3 fC used during the first experiment due to limitations of the FEB itself.

Finally, it was decided to use the same PMTs than in the first experiment as trigger. This time, they were placed on their narrow side to only cover an area on the detector smaller than three strips. On the data acquisition side, no DAQ software was available yet at the time of experimentation

and scalers were once again used. As can be seen from Figure 6.11, the pulse processing has been inspired by the previous scheme. Thanks to the lower number of channels to monitor, the cluster size could be estimated by counting the signals on single channels (A, B and C on their own) but also on groups of two (A and B, B and C) and three channels (A and B and C) in coincidence with the trigger.

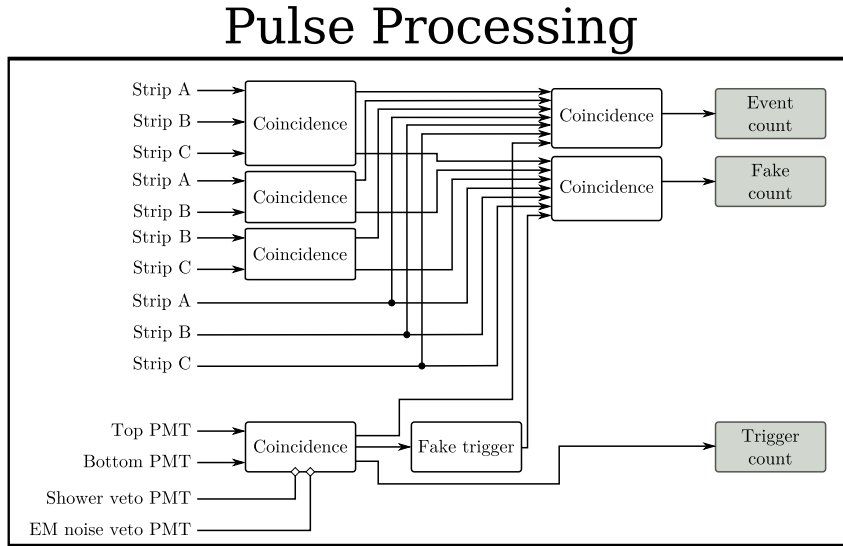


Figure 6.11: Similarly to Figure 6.8c, the signals are counted in coincidence with the trigger signals provided by PMTs. To estimate the cluster size, the channels are counted by groups of three, two but also alone.

The results of the second round of tests with INFN preamplifiers are presented in Figure 6.12 and Table 6.2. These results are consistent with what was measured with the first tested prototypes. The efficiency sigmoid has been measured once again with the CMS FEB, using a threshold of 170 fC and is in agreement with the data collected in 2013. The performance of the detector with the preamplifiers tuned at 7.2 and 6.4 fC falls in the very same values than the setting at 7 fC according to the table. A maximum shift of 410 V is observed for a threshold of 5 fC.

With the care placed into having a good grounding of the setup as well as a good impedance matching, the noise rate per unit area is this time lower than what previously measured. Nevertheless, it still is more than one order of magnitude higher than in the case of the CMS FEB with a threshold set at 170 fC. The noise rate is measured to be at lowest around 0.7 Hz/cm² when measured to be approximately 0.05 Hz/cm² for the CMS FEB. At such high threshold values, the noise rate per unit area is not expected to vary much. The data collected at the RPC assembly laboratory then displays much better data taking conditions with both electronics.

Finally, the cluster size is measured to be similar for both electronics at the level of the working point and is in between 2.2 and 2.4 strips on average. The spatial resolution of both devices would then be the same.

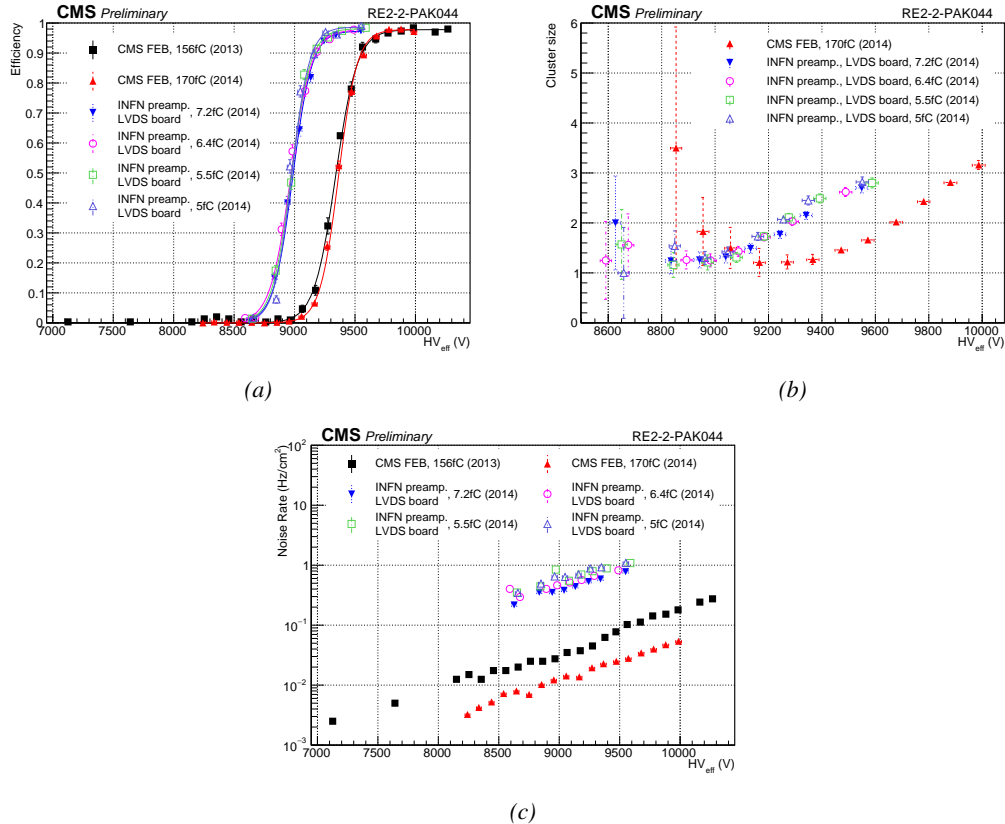


Figure 6.12: Efficiency (Figure 6.12a), cluster size (Figure 6.12b) and noise rate per unit area (Figure 6.12c) of the CMS RE2-2 detector tested with the standard CMS FEBs (black and red) and with the INFN preamplifier mounted onto the CMS FEB at different thresholds (blue, pink, green and purple).

Data	ϵ_{max}	$\lambda \cdot 10^{-2} \text{ V}^{-1}$	HV_{50} (V)	ϵ_{WP}	HV_{WP} (V)
CMS FEB, 156fC (2013)	(0.978 ± 0.004)	(1.12 ± 0.07)	(9339 ± 11)	(0.97 ± 0.01)	(9752 ± 27)
CMS FEB, 170fC (2014)	(0.978 ± 0.003)	(1.30 ± 0.06)	(9364 ± 9)	(0.97 ± 0.01)	(9740 ± 19)
INFN/CMS FEB, 7.2fC (2014)	(0.973 ± 0.006)	(1.26 ± 0.09)	(8985 ± 10)	(0.97 ± 0.01)	(9368 ± 26)
INFN/CMS FEB, 6.4fC (2014)	(0.978 ± 0.007)	(1.16 ± 0.08)	(8969 ± 11)	(0.97 ± 0.01)	(9372 ± 28)
INFN/CMS FEB, 5.5fC (2014)	(0.981 ± 0.005)	(1.26 ± 0.09)	(8973 ± 12)	(0.97 ± 0.01)	(9357 ± 28)
INFN/CMS FEB, 5fC (2014)	(0.987 ± 0.004)	(1.37 ± 0.10)	(8976 ± 12)	(0.98 ± 0.01)	(9342 ± 28)

Table 6.2: Results of the sigmoid fit (Formula 3.24) performed on the data presented in Figure 6.12a. The working point and its corresponding efficiency are computed using Formulas 3.24 and 3.25.

4636 In addition to the tests performed on the electronics with the CMS RPC, the electronics also
 4637 have been tested on a gRPC designed in Ghent. The gRPC used for this experiment is described
 4638 in Figure 6.13. The detector, showed on Figure 6.14, uses a double-gap layout with float glass
 4639 electrodes of 1.1 mm and a gas gap of 1.2 mm. The electrodes themselves are made out of four
 4640 pieces of glass glued together. Such a design was studied for high-rate detection purposes and aimed
 4641 to serve as a proof of concept for RPCs built using small pieces assembled together to produce
 4642 a larger detection area. Indeed, in the context of R&D in the field of high-rate RPCs, most low
 4643 resistivity materials are custom made doped glass or ceramics plates. These materials can't be

⁴⁶⁴⁴ produced in large areas as they are not manufactured on a large enough scale. Thus, building large
⁴⁶⁴⁵ detectors requires using such methods.

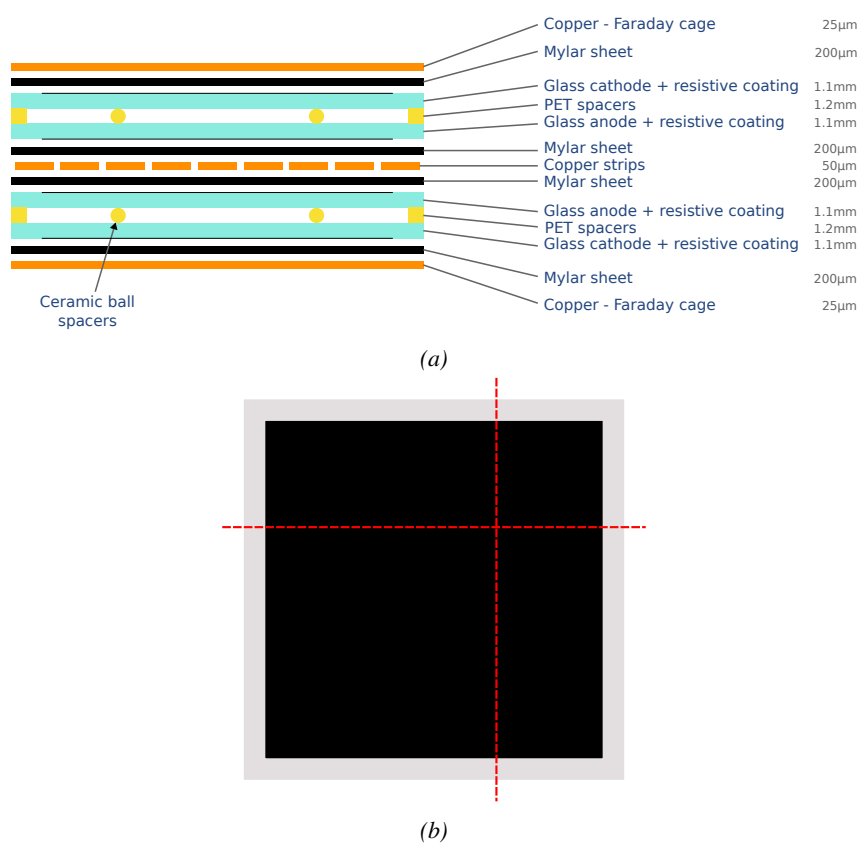


Figure 6.13: The glass RPC developed by Ghent uses a double-gap design (Figure 6.13a). The electrodes are made of four pieces of float glass glued into a single plate (Figure 6.13b). Indeed a gluing technique has been investigated as most new low resistivity materials foreseen for RPCs of the new generation are not available in large areas.

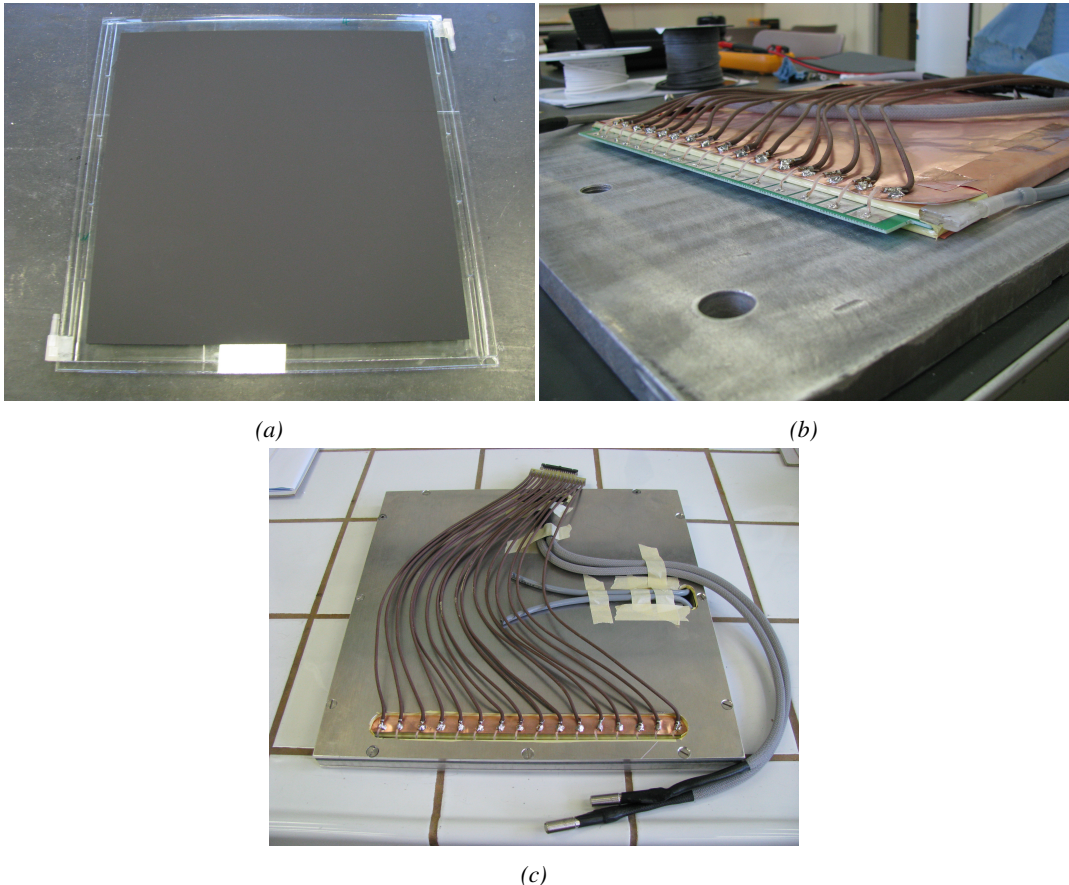


Figure 6.14: Figure 6.14a: A gap used to conceive the gRPC tested at CERN. Figure 6.14b: Both gaps with their read-out panel are placed into a faraday made out of copper. Figure 6.14c: The faraday cage containing the double-gap gRPC is finally placed into its aluminium case.

4646 The tests involving this detector were conducted in 2015 with the setup described by Figure 6.15.
 4647 The photomultipliers used to trigger the data taking were a little larger than the detector and the strips
 4648 themselves. Similarly to the case of the GIF experiment described in Section 5.2.2 of Chapter 5, it
 4649 has been necessary to evaluate the geometrical acceptance of the setup to detect cosmic muons.
 4650 This way, a C++ Monte Carlo simulation has been written using the dimensions of the experimental
 4651 setup. By running 1000 simulations in which a million muons were generated in a source plane much
 4652 larger than the experimental setup itself to reach high zenith angles, the geometrical acceptance was
 4653 measured to be (0.9835 ± 0.0014) . This factor has then been used to correct the measured efficiency
 4654 of the detector.

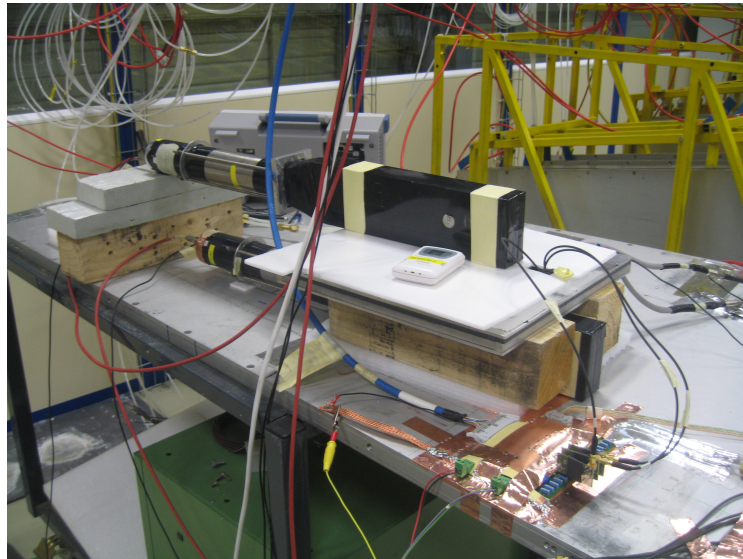


Figure 6.15: Experimental setup used to test the INFN preamplifier mounted on the CMS like FEB with the glass RPC build by Ghent.

4655 Thanks to the activities ongoing for the preparation of the CMS RPC experiment taking place
 4656 at GIF++ and detailed in Chapter 5, a first prototype of DAQ software was available to automate
 4657 the data tacking process. Thanks to this early version of the software, the pulse processing was
 4658 made more simple. The three channels connected to the preamplifiers were sent directly into a
 4659 V1190A TDC manufactured by CAEN. The trigger was provided by the same trigger pulse process-
 4660 ing described in Figure 6.11. The output of the coincidence of both scintillators was sent into the
 4661 *TRIGGER* input of the TDC. The communication with the computer was done thanks to a V1718
 4662 module. More details on the DAQ can be found in Appendix A. Contrary to the data now collected
 4663 at GIF++, the output of the first DAQ script consisted in a simple text file using a format described
 4664 in Source Code 6.1. The analysis is then performed using a loop through the data file.

```

Evt0      nHits
ChHit1    THit1
ChHit2    THit2
ChHit3    THit3
ChHit4    THit4
ChHit5    THit5
4665 ...
Evt1      nHits
ChHit1    THit1
ChHit2    THit2
ChHit3    THit3
...
  
```

4666 *Source Code 6.1: Description of the format used to store the data collected during the experiment aiming at
 testing the INFN electronics with a gRPC built by Ghent. For each trigger received in the TDC module, an
 event is created. A first line containing two columns is written in the output file with the event number EvtX
 and the recorded number of hits nHits. This line is directly followed by the list of hits in each channel ChHitX
 and their corresponding time stamp THitX organized into two columns.*

The results of the experiment with the gRPC are provided in Figure 6.16 and Table 6.3. The efficiency of the detector reaches 95% at working voltage, indicating that such a detector using electrodes composed of several glued pieces can be an option for the future of RPC technologies. The benefits of the preamplifiers is once again visible through the huge efficiency shift towards lower voltages. The shift reaches almost 470 V for thresholds lower than 6 fC.

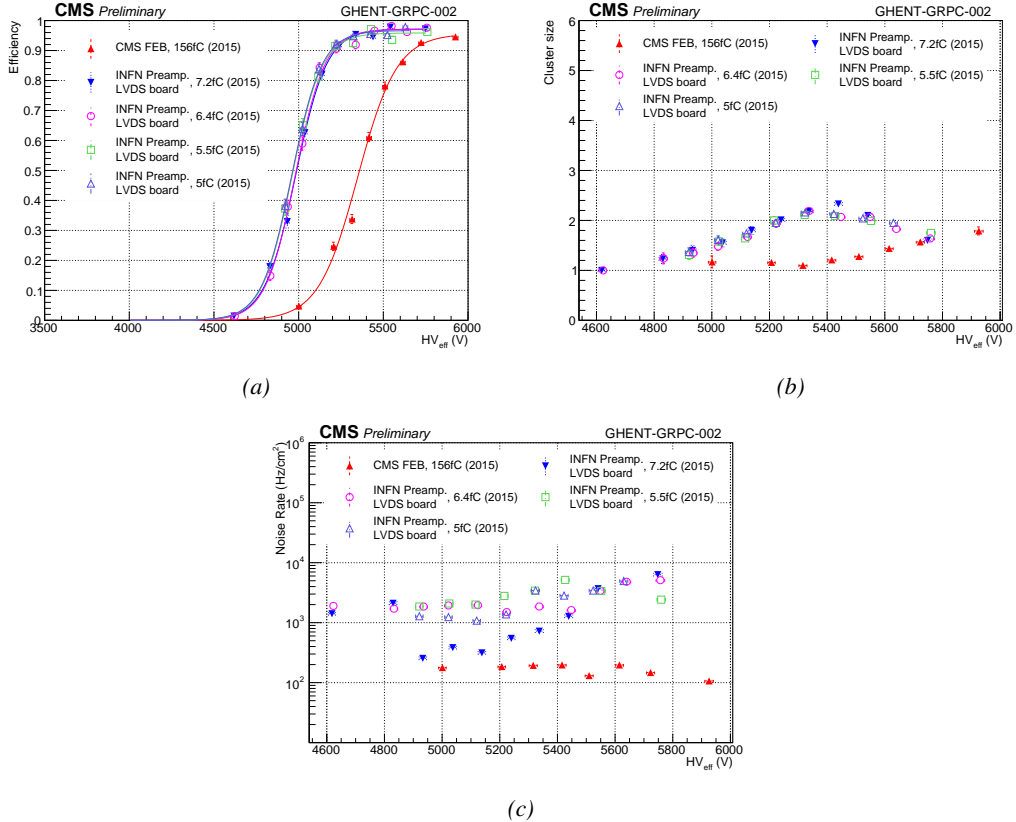


Figure 6.16: Efficiency (Figure 6.16a), cluster size (Figure 6.16b) and noise rate per unit area (Figure 6.16c) of the Ghent gRPC detector tested with the standard CMS FEBs (red) and with the INFN preamplifier mounted onto the CMS FEB at different thresholds (blue, pink, green and purple).

Data	ϵ_{max}	$\lambda \cdot 10^{-2} \text{ V}^{-1}$	HV_{50} (V)	ϵ_{WP}	HV_{WP} (V)
CMS FEB, 156fC (2015)	(0.956 ± 0.007)	(0.86 ± 0.04)	(5349 ± 8)	(0.94 ± 0.01)	(5839 ± 23)
INFN/CMS FEB, 7.2fC (2015)	(0.972 ± 0.006)	(1.09 ± 0.06)	(4983 ± 8)	(0.96 ± 0.01)	(5403 ± 22)
INFN/CMS FEB, 6.4fC (2015)	(0.971 ± 0.005)	(1.13 ± 0.06)	(4981 ± 8)	(0.96 ± 0.01)	(5391 ± 22)
INFN/CMS FEB, 5.5fC (2015)	(0.959 ± 0.006)	(1.13 ± 0.11)	(4960 ± 11)	(0.95 ± 0.02)	(5371 ± 37)
INFN/CMS FEB, 5fC (2015)	(0.967 ± 0.006)	(1.12 ± 0.11)	(4959 ± 11)	(0.96 ± 0.02)	(5371 ± 38)

Table 6.3: Results of the sigmoid fit (Formula 3.24) performed on the data presented in Figure 6.16a. The working point and its corresponding efficiency are computed using Formulas 3.24 and 3.25.

The cluster size also shows a shift but its value suddenly decreases after 5.4 kV. After a rise above 2, the cluster size drops when the detector reaches the plateau. A first idea to explain this

phenomenon would be to check the cluster algorithm to make sure that it is not biased and does not introduce a fake split of the clusters due to arbitrarily strict selection rules. Clusters are always made of neighbour strips getting a hit within a certain time window. In the algorithm written to analyse the data, it is required for the maximum time difference between the earliest hit and the latest hit in a cluster to be smaller than 10 ns. Physically, assuming of drift velocity of the electrons in the gas of the order of 0.1 mm/ns [286], the growth of an avalanche only takes a few ns. This effect is visible in Figure 6.17a in which the maximum time difference has been artificially increased to 300 ns. The peak reveals that the avalanches are not expected to grow over a time period longer than 10 ns. No peak emerges at time differences longer than 10 ns indicating that the choice of a short time development within the algorithm was justified. This conclusion is supported by Figure 6.17b in which the evolution of the reconstructed cluster size with increasing maximum time difference shows no effect.

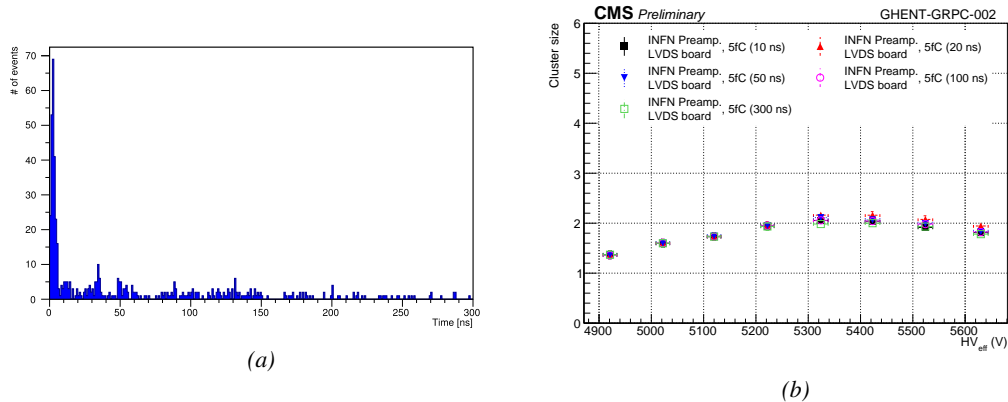


Figure 6.17: Figure 6.17a: Time difference between the first and last hit composing a cluster in the gRPC. The maximum time difference is set to 300 ns. Figure 6.17b: Variation of the reconstructed average cluster size as a function of the time constraint used in the algorithm.

Due to the available number of channels, the cluster size is limited to 3. It is reasonable to assume that this only is the cause of the fall of cluster size beyond 5.4 kV. Indeed looking closely at both Figure 6.18 and Figure 6.19, the link between increasing HV and decreasing cluster size can be understood. On the one hand, Figure 6.18 indicates that the cluster size features at first a maximum at 1. The maximum moves then from 1 to 3 over the points at 5120 V, 5222 V and 5324 V. Then over the last three voltage points, the bin at 2 drops to the profit of the bin at 1, the bin at 3 staying more or less stable. On the other hand, Figure 6.19 provides us more information about the localisation of the clusters among the three read-out strips. At the lowest two voltages, most of the data is contained in the central strip. At 5120 V, the highest bin is the one corresponding to the central strip with a cluster size of 1. Already at 5222 V, the balance changes towards the central strip with 3 strips in the clusters. At 5324 V, even more events happen with clusters of all 3 strips while the events with a single hit in the side strips starts to increase. The number of events with cluster made of all 3 strips will not vary much anymore while the number of events with clusters made of 2 strips will decrease and the single hits in the side strips will continue rising. This information indicates that the avalanches in the gap start to get stronger. Indeed, the increase of the events containing single hits mainly increases on the side strips points to an intensification of the avalanche gain on the strip adjacent to the three channels connected to the read-out setup. Only a single hit is read-out while

in reality this was the contribution of bigger avalanches. The events with clusters of size 2 tend to decrease due to the stronger gain that should normally be triggering wider avalanches. The cluster size distribution of Figure 6.18 gives the impression that the distribution is moving towards higher values but the geometrical limitation of the system due to the very low number of channels makes it impossible to measure.

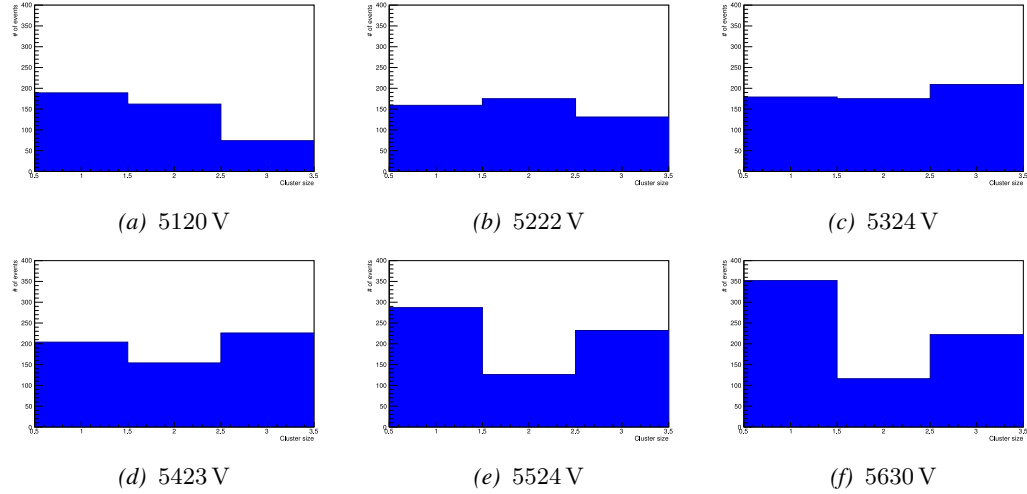


Figure 6.18: Evolution of the cluster size distribution with increasing voltage for the gRPC tested with the INFN preamplifiers using a threshold of 5 fC.

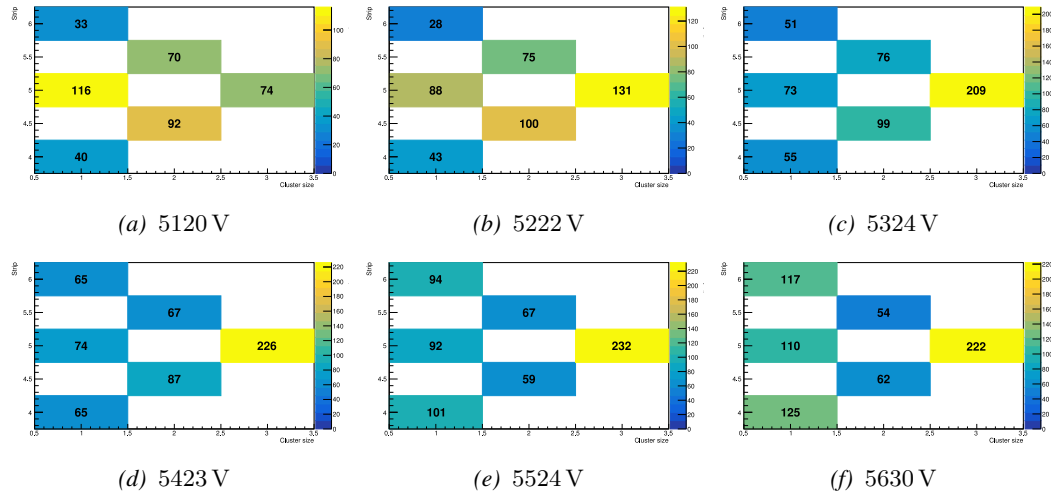


Figure 6.19: Map of the cluster size distribution as a function of the cluster position with increasing voltage for the gRPC tested with the INFN preamplifiers using a threshold of 5 fC.

Eventhough the performance of the detector are promising, the results concerning the noise rate per unit area seem to indicate that the detector and its combination with the electronics in the case of this experiment produces very high levels of noise, if compared to the noise measured in the RE4

4711 detector. With each type of electronics, the noise doesn't indicate a clear correlation with increasing
 4712 voltage. The hypothesis at this stage would be that the noise is not created inside of the gas volume by
 4713 avalanches triggered along the glueing lines, where the electric field could be abruptly perturbed.
 4714 It would rather come from the read-out channel itself, and from its connection to the electronics.
 4715 Indeed, looking at the noise profile measured in the detector and presented in Figure 6.20a, it is clear
 4716 that the noise is localised in two areas corresponding to the HV connectors in the case of the HV
 4717 scan performed with the CMS FEB. Moreover, contrary to the very careful work performed on the
 4718 RE2 chamber to match the impedance of the strips with the read-out cables connected to the board
 4719 on which the INFN preamplifiers are mounted, no matching was done on the gRPC due to a lack
 4720 of time. The noise measured in the tested three channels is showed in Figure 6.20b. This region of
 4721 the detector doesn't correspond to the HV connectors according to Figure 6.20a. Nevertheless, the
 4722 number of hits counted in the detector is much higher than in the CMS FEB case. Looking more
 4723 carefully to Figure 6.21 presenting the hit time profile in both cases together with the time profile of
 4724 the CMS RE2-2 detector tested with INFN preamplifiers, it is clear that the detector is noisier. Also,
 4725 the reflections due to the impedance mismatch is clearly visible in Figure 6.21b.

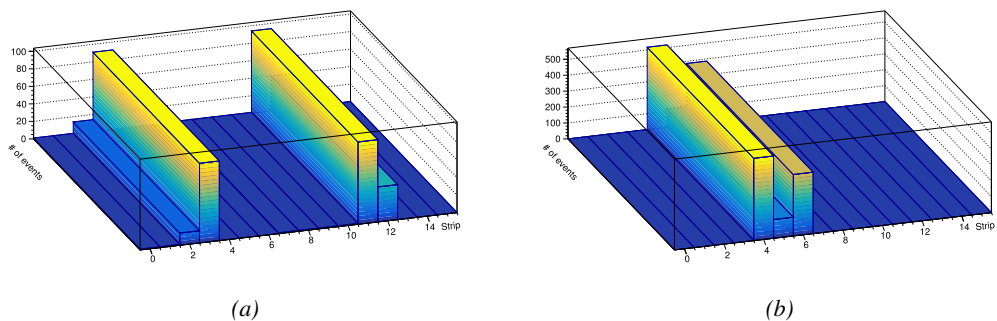


Figure 6.20: Noise profile measured in the glass RPC built by Ghent tested with the standard CMS FEB (Figure 6.20a) and the INFN preamplifiers mounted on a CMS-like FEB (Figure 6.20b).

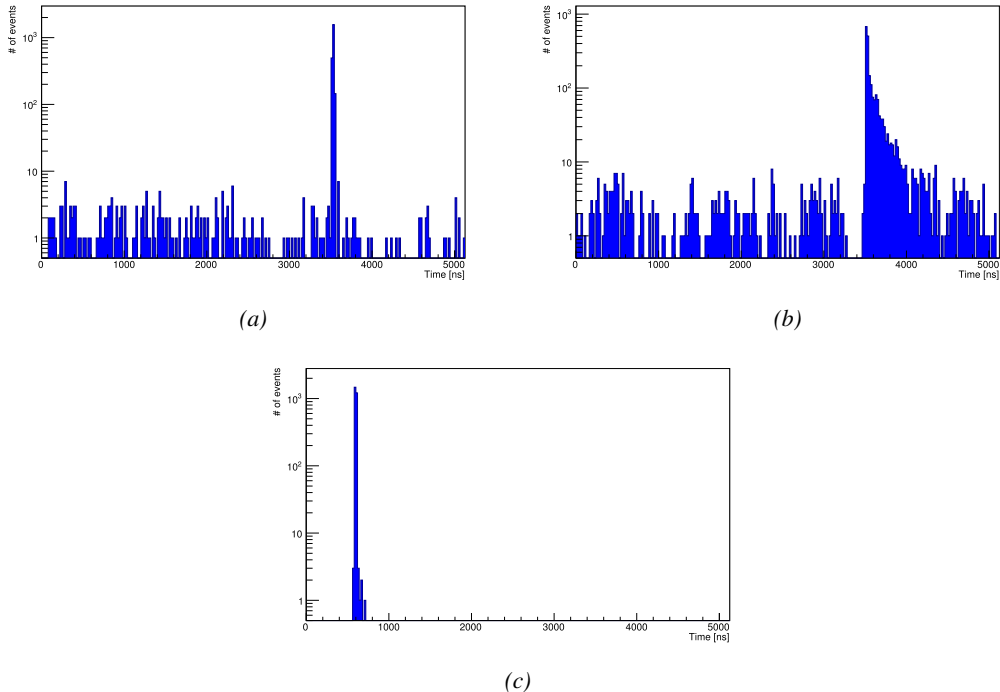


Figure 6.21: The arrival time of the hits recorded in the gRPC tested with the CMS FEB (Figure 6.21a) and with the INFN preamplifiers (Figure 6.21b), and recorded in the CMS RE2 RPC tested with the INFN preamplifiers (Figure 6.21c).

6.2.3 HARDROC 2 based RPC read-out

The HAdronic RPC Digital Read-Out Chip (HARDROC) ASIC, as its name suggests, has been developed for RPC applications and in particular for the read-out RPCs of the Semi-Digital HCAL (SDHCAL) that is being studied in the perspective of the International Linear Collider (ILC). The SDHCAL detectors are required to have a high granularity compared to the CMS RPCs and hence, they use 1 cm² read-out pads instead of strips. This choice results in a huge number of channels. The ASIC is mounted directly on the read-out pannel for compactness as can be seen in Figure ?? and feature three thresholds to provide a semi-digital information.

The PETIROC that inspired the CMS RPCROC uses a similar technology than the one developed for the HARDROC and is manufactured by the same company. It is safe to conclude that the preliminary results obtained with the HARDROC electronics constitute a strong indication on the potential performance of a FEB developed specifically for CMS detectors. The leading institute in the development of the SDHCAL based on single-gap glass RPCs (gRPCs) is the Institut de Physique Nucléaire de Lyon (IPNL) which also played a great role in developing iRPCs for CMS.

A read-out pannel using the HARDROC 2 technology was lended by this institute and was tested onto a CMS RPC. Contrary to the tests with the INFN preamplifiers that were made using an RE2-2 CMS RPC built in 2007 for the second endcap disk of CMS, the choice was made to use an RE4-3 detector built during LS1 to equip the fourth endcap. Indeed, the pannel can't be sandwiched between two RPC gaps due to the embedded electronics and a single CMS RPC gap was used. At the time of this experiment, only RE4-3 gaps were available and the choice was made to change

4746 detector with respect to the previous series of tests conducted on the INFN preamplifiers. As for
 4747 the INFN preamplifiers, the pannel has been tested on the gRPC built by UGent. The gRPC being
 4748 smaller than the HARDROC read-out that was used for the experiment but thanks to the 2D read-out
 4749 using pads, this was not a problem for the data acquisition.



(a)

(b)

Figure 6.22: Experimental setups used to test the HARDROC2 electronics with a CMS RE4-3 gap (Figure 6.22a) and a gRPC gap built in Ghent (Figure 6.22b).

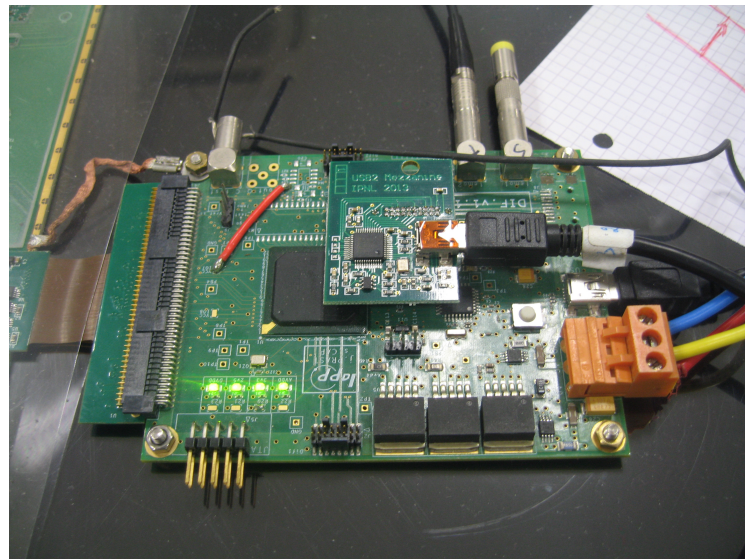


Figure 6.23: HARDROC2 control chip with its "Mezzanine" used to collect the data from the different HARDROC ASICs and communicate with the computer. On top of the picture, the trigger is brought by a coaxial cable. The connection with the computer is assured by both the USB cables.

4750 Once again, the experiment was conducted in the CMS RPC assembly laboratory at CERN and
 4751 the setups are shown in Figure 6.22. The read-out panel is placed directly on top of the gaps and
 4752 pressed against the detector surface thanks to weights. The same PMTs are used to provide a trigger

to the data acquisition. In the particular case of the HARDROC 2 electronics, the output signal does not correspond to the LVDS signals provided by the CMS FEB. Moreover, there would be more than 1500 channels to constantly monitor and unfortunately, there would not be enough VME TDC modules to use with the DAQ software designed for the experiment involving the INFN preamplifiers. Nevertheless, a custom-made DAQ software was designed by the members of IPNL's team to read-out the electronics through the chip presented in Figure 6.23. The data is stored in the buffer of the ASIC continuously and dumped into the computer when a trigger is signal is received.

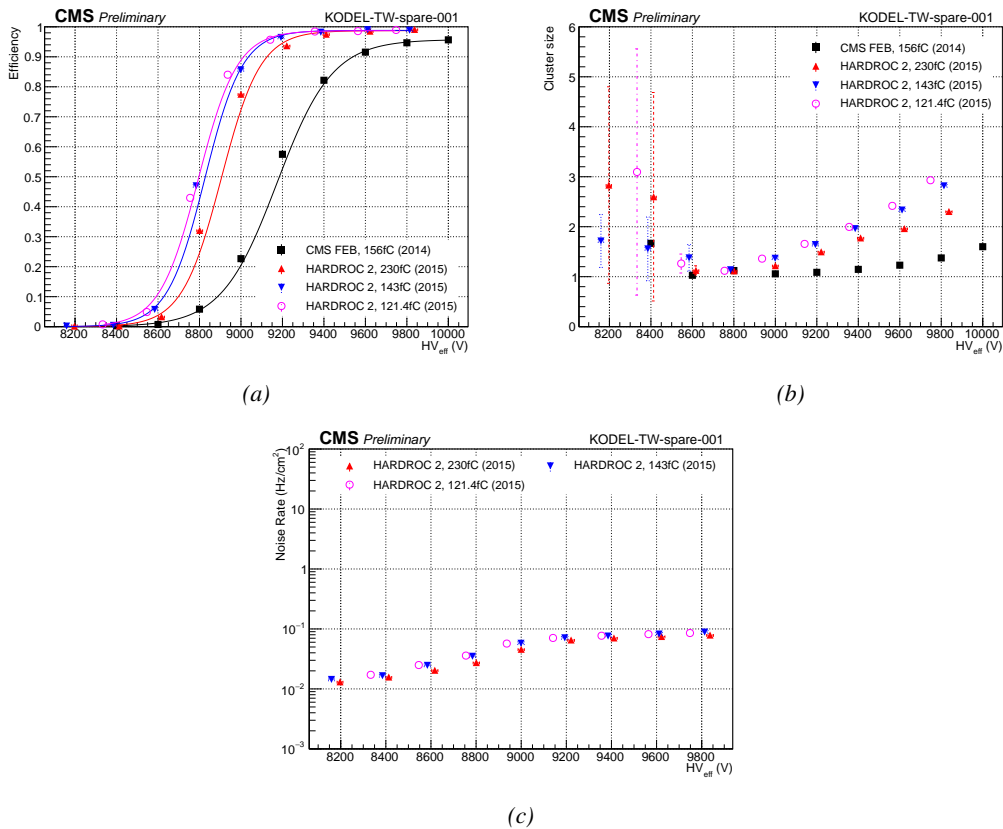


Figure 6.24: Efficiency (Figure 6.24a), cluster size (Figure 6.24b) and noise rate per unit area (Figure 6.24c) of the CMS RE4-3 detector tested in single gap mode with the standard CMS FEBs (black) and with the HARDROC 2 readout panel at different thresholds (red, blue and pink).

Data	ϵ_{max}	$\lambda \cdot 10^{-2} \text{ V}^{-1}$	HV_{50} (V)	ϵ_{WP}	HV_{WP} (V)
CMS FEB, 156fC (2014)	(0.958 ± 0.000)	(0.75 ± 0.00)	(9174 ± 1)	(0.94 ± 0.00)	(9716 ± 2)
HARDROC 2, 230fC (2015)	(0.987 ± 0.002)	(1.06 ± 0.04)	(8905 ± 8)	(0.98 ± 0.01)	(9333 ± 17)
HARDROC 2, 143fC (2015)	(0.988 ± 0.001)	(1.10 ± 0.04)	(8826 ± 8)	(0.98 ± 0.01)	(9243 ± 17)
HARDROC 2, 121.4fC (2015)	(0.987 ± 0.001)	(1.07 ± 0.04)	(8795 ± 8)	(0.98 ± 0.01)	(9220 ± 17)

Table 6.4: Results of the sigmoid fit (Formula 3.24) performed on the data presented in Figure 6.24a. The working point and its corresponding efficiency are computed using Formulas 3.24 and 3.25.

The results of the tests conducted with the HARDROC 2 on a CMS gap are presented in Fig-

ure 6.24 and Table 6.4. These results can hardly be compared to what was measured with the INFN preamplifiers as the detector was not tested using the single-gap mode. The tested thresholds are high compared to the ones displayed by the INFN preamplifiers and are of the order of magnitude of the current CMS FEB. Nevertheless, the performance of the detector equipped with this read-out pannel is measured to be better. Indeed, a shift of 400 to 500 V is observed at thresholds ranging from 230 to 121.4 fC. [Here it could be nice to bring an explanation to this observation.]

The cluster size is provided for information as a direct comparison of the cluster size measured with 1 cm^2 pads and long copper strips with width of a few cm is not possible. The measured cluster size at working voltage with the CMS FEB is consistent with what would be expected of a single-gap RPC. Indeed, the usage of two gaps in an OR system allows for a stronger overall gain and hence, the cluster size is greater. A more precise estimation of the charge spread inside of the gap is obtained using pads instead of strips. At working voltage, an avalanche is detected within less than two pads on average. An extra information could be used to further improve the spatial resolution of the detector. Indeed, as stated in the introduction of the Section, the HARDROC 2 is a semi-digital electronics and features three threshold levels. Tuning these thresholds would lead to an approximation of the induced charge profile over the neighbouring pads. A gaussian fit over the digitized distribution would give an estimation of the position of the avalanche center.

Finally, the noise measured in the electronics is of the same order of what had been measured in Figure 6.12c. It is safe to assume that the noise level in the case of a single-gap RPC is expected to be of the same order of magnitude than its double-gap counterpart as the noise mainly is electromagnetic. Figure 6.25 provides a clearer understanding of the position of the trigger PMTs and of the noise measured with the HARDROC. The noise of the electronics itself is very small and the read-out pannel is sensitive enough to measure the noise in the RPC gap. Indeed, except for a few visible hot spots, the observed noise profile corresponds perfectly to the spacer positions inside of the gap volume. The PET buttons used to maintain the uniformity of the gas volume cause noise at their proximity as they modify the local electric field.

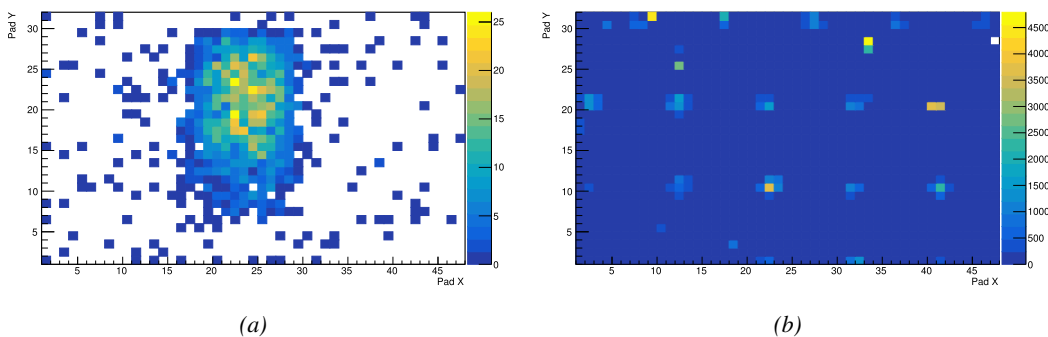


Figure 6.25: Measured muon (Figure 6.25a) and noise (Figure 6.25a) profiles in the read-out pads of the HARDROC 2 over a CMS RE4-3 gap. The inner structure of the gap and the presence of the spacers in the volume is visible.

The results of the experiment with the gRPC are provided in Figure 6.26 and Table 6.5. Unfortunately the gRPC had not been tested in single gap mode with the CMS FEB. Thus, a direct comparison is not possible as the data were not collected in similar conditions. The detector could only be tested with a single HARDROC 2 threshold setting (143 fC). As for the double-gap, the effi-

4791 efficiency of the single-gap reaches 95% at working voltage. The working voltage is consistent with the
 4792 double-gap detector operated with the CMS FEB indicating that the HARDROC is more sensitive to
 4793 lower charges. The difference in efficiency rising is consistent with the use of one gap versus two in
 4794 the case of the CMS FEB.

4795 As discussed in the case of the CMS RE4-3 gap, the direct comparison of the cluster sizes is
 4796 not possible. In this sense, the proximity of both results only is fortuitous. The cluster size of
 4797 approximately 1.6 measured with the HARDROC 2 at working voltage is of the same order than
 4798 what had previously been measured for the CMS gap indicating that at equivalent performance, the
 4799 gain and hence, the induced charge could be comparable.

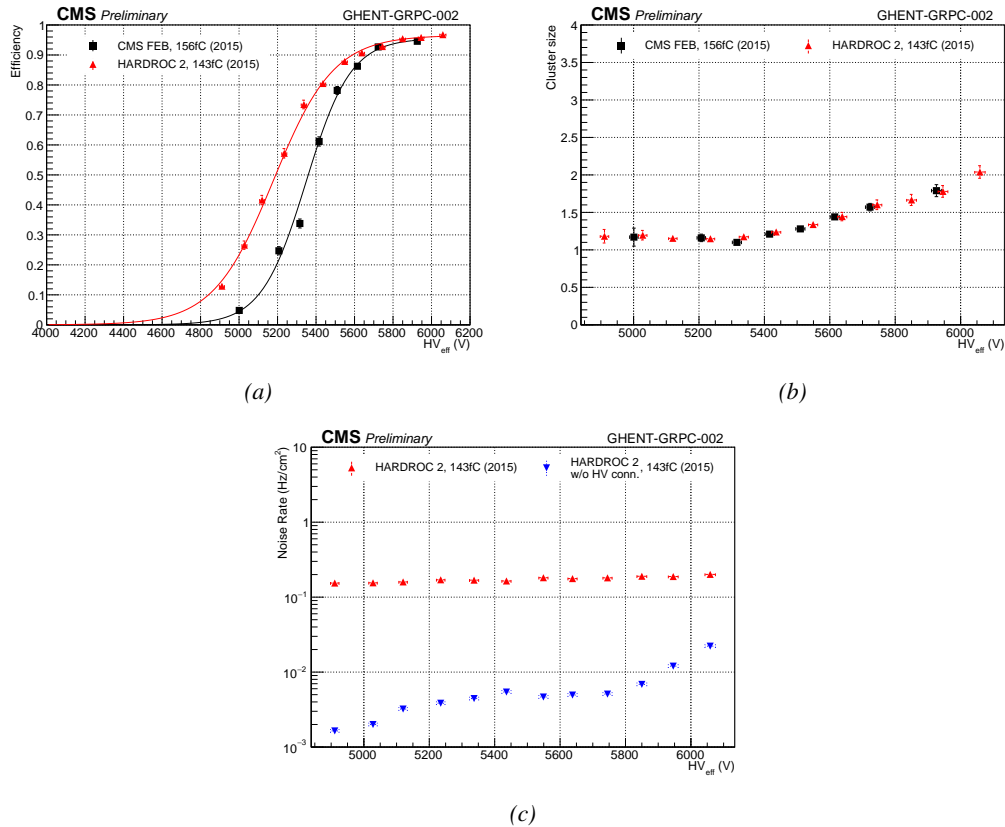


Figure 6.26: Efficiency (Figure 6.24a), cluster size (Figure 6.24b) and noise rate per unit area (Figure 6.24c) of the UGent gRPC tested in double-gap mode with the standard CMS FEBs (black) and in single-gap with the HARDROC 2 readout panel at a threshold of 143 fC.

Data	ϵ_{max}	$\lambda \cdot 10^{-2} \text{ V}^{-1}$	HV_{50} (V)	ϵ_{WP}	HV_{WP} (V)
CMS FEB, 156fC (2015)	(0.956 ± 0.007)	(0.86 ± 0.04)	(5349 ± 8)	(0.94 ± 0.01)	(5839 ± 23)
HARDROC 2, 143fC (2015)	(0.966 ± 0.004)	(0.64 ± 0.02)	(5179 ± 7)	(0.95 ± 0.01)	(5790 ± 25)

Table 6.5: Results of the sigmoid fit (Formula 3.24) performed on the data presented in Figure 6.26a. The working point and its corresponding efficiency are computed using Formulas 3.24 and 3.25.

4800 Finally, the noise measured in the electronics seemed higher than in the case of the CMS gap.

4801 Looking closer to the noise profile provided in Figure 6.27, it can be seen that the noise measurement
 4802 was affected by the HV connector. Indeed, the high noise measured in pads 41 and 42 along X and 22
 4803 to 25 along Y, corresponds exactly to the position of the HV connector on the cathode side. Contrary
 4804 to the case of the CMS gap were the HV connector was far from the read-out area, the gRPC is
 4805 smaller than the read-out and due to the poor grounding of the setup the electric field created by
 4806 the HV connector could affect the read-out. Excluding the corresponding pads gives a much more
 4807 reliable noise measurement as can be seen in Figure 6.26c. Through the noise profile, a better
 4808 understanding of the gRPC uniformity can be obtained. First of all, the row corresponding to Y=16
 4809 seem consistently noisier than the neighbouring pads and could correspond to the glueing line that lies
 4810 along this pad row. The noise increase along this line is not very clear though and no corresponding
 4811 behaviour can be observed along the other glueing line along column X=30. But the gas volume
 4812 corresponding to the largest glass plate, spreading from columns 31 to 47 along X and rows 1 to 15
 4813 clearly shows a stronger noise in its center. The detection area being small, only a few ceramic ball
 4814 spacers were used to maintain the distance in between the electrodes. It is not impossible that the ball
 4815 spacer located in the center of this volume popped out. Due to the absence of a spacer, the force
 4816 applied by electric field onto the electrodes could have made the distance in between the electrodes
 4817 smaller and artificially increased the observed electric field, also increasing the measured noise.

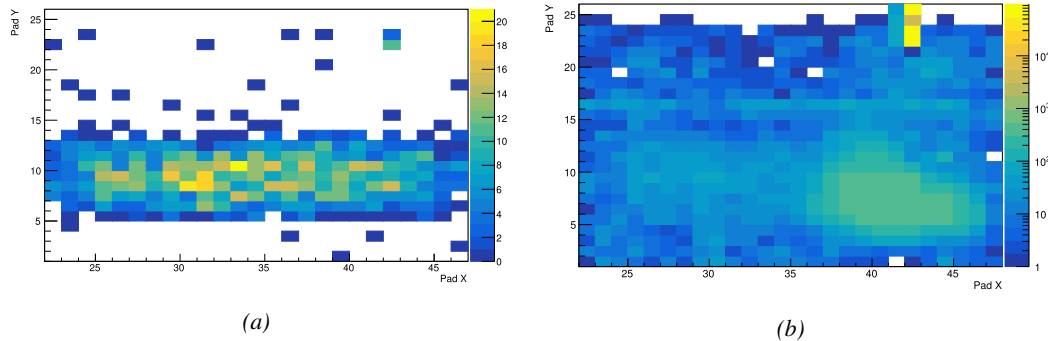


Figure 6.27: Measured muon (Figure 6.27a) and noise (Figure 6.27a) profiles in the read-out pads of the HARDROC 2 over a gRPC gap built by Ghent.

4818 6.2.4 Outlooks and current FEE certification status

